Seasonal Relationships between Large-Scale Climate Variability and Antarctic Sea Ice Concentration

GRAHAM R. SIMPKINS AND LAURA M. CIASTO

Climate Change Research Centre, University of New South Wales, Sydney, New South Wales, Australia

DAVID. W. J. THOMPSON

Department of Atmospheric Science, Colorado State University, Fort Collins, Colorado

MATTHEW H. ENGLAND

Climate Change Research Centre, University of New South Wales, Sydney, New South Wales, Australia

(Manuscript received 17 June 2011, in final form 9 January 2012)

ABSTRACT

The observed relationships between anomalous Antarctic sea ice concentration (SIC) and the leading patterns of Southern Hemisphere (SH) large-scale climate variability are examined as a function of season over 1980–2008. Particular emphasis is placed on 1) the interactions between SIC, the southern annular mode (SAM), and El Niño–Southern Oscillation (ENSO); and 2) the contribution of these two leading modes to the 29-yr trends in sea ice. Regression, composite, and principal component analyses highlight a seasonality in SH sea ice–atmosphere interactions, whereby Antarctic sea ice variability exhibits the strongest linkages to the SAM and ENSO during the austral cold season months. As noted in previous work, a dipole in SIC anomalies emerges in relation to the SAM, characterized by centers of action located near the Bellingshausen/Weddell and Amundsen/eastern Ross Seas. The structure and magnitude of this SIC dipole is found to vary considerably as a function of season, consistent with the seasonality of the overlying atmospheric circulation anomalies. Relative to the SAM, the pattern of sea ice anomalies linked to ENSO exhibits a similar seasonality but tends to be weaker in amplitude and more diffuse in structure. The relationships between ENSO and sea ice also exhibit a substantial nonlinear component, highlighting the need to consider both season and phase of the ENSO cycle when diagnosing ENSO–SIC linkages. Trends in SIC over 1980–2008 are not significantly related to trends in either the SAM or ENSO during any season, including austral summer when the trend in the SAM is most pronounced.

1. Introduction

Sea ice has the potential to modify Earth's climate system through a variety of factors. For example, it can perturb the radiation budget through the ice–albedo feedback, modify deep-water production and thus the global overturning circulation, and control air–sea exchanges of heat, moisture, and carbon. In addition to the physical impacts, changes in sea ice also have significant ecological implications. As such, understanding the mechanisms that govern sea ice variability is of crucial importance, particularly in light of contemporary changes to the polar climate systems. In the Arctic, sea ice extent (SIE; defined here as the cumulative area with at least 15% sea ice cover) has experienced an extremely rapid decline in the past 30 years (e.g., Comiso and Nishio 2008) at a rate that few individual model simulations of contemporary climate have been able to capture (Stroeve et al. 2007). By contrast, hemispheric-scale Antarctic SIE has exhibited a modest increase of $\sim 1.0 \pm 0.4\%$ decade^{-1} over 1979–2006 (Comiso and Nishio 2008; Cavalieri and Parkinson 2008). Most coupled climate models are unable to capture the correct sign of these changes in Southern Hemisphere (SH) SIE (Stroeve et al. 2007), prompting questions regarding

Corresponding author address: Graham Simpkins, Climate Change Research Centre, University of New South Wales, Sydney NSW 2052, Australia.
E-mail: g.simpkins@unsw.edu.au

DOI: 10.1175/JCLI-D-11-00367.1

© 2012 American Meteorological Society

the extent to which the physical mechanisms driving Antarctic sea ice variability are understood. In this study, both trends and interannual variability in Antarctic sea ice are examined, focusing on the atmospheric circulation associated with the leading patterns of climate variability.

The SH atmospheric circulation is dominated by two modes of variability—the southern annular mode (SAM) and the high-latitude response to El Niño–Southern Oscillation (ENSO), which are hereafter qualified as the leading patterns of SH large-scale climate variability. The SAM is characterized by near zonally symmetric north–south vacillations in the position of the midlatitude westerly jet (Karoly 1990; Hartmann and Lo 1998; Thompson and Wallace 2000). The high index polarity of the SAM describes a poleward displacement of the jet associated with negative (positive) pressure anomalies over the high (mid) latitudes. The SAM also possesses a significant nonannular component, expressed as a region of locally enhanced pressure anomalies over the Amundsen Sea (e.g., Thompson and Wallace 2000).

In contrast, the SH high-latitude atmospheric response to ENSO is characterized by a wavelike structure (Karoly 1989). During El Niño conditions, increased convection in the central tropical Pacific gives rise to anomalous upper-level vorticity, exciting a pattern of stationary Rossby waves that propagate to the extratropical SH (e.g., Hoskins and Karoly 1981). The resulting wave train is manifested as cyclonic anomalies off western New Zealand, anticyclonic anomalies over the Amundsen Sea, and cyclonic anomalies off the east coast of South America (Karoly 1989; Mo and Higgins 1998; Garreaud and Battisti 1999). The wave train bears strong resemblance to the first Pacific–South American (PSA) pattern (e.g., Karoly 1989; Mo 2000), and thus the physical impacts of ENSO and the PSA on the SH climate are similar. It should be noted that during austral summer, the extratropical atmospheric circulation associated with ENSO exhibits greater zonal symmetry, and thus projects more strongly onto the SAM (Karoly 1989; L'Heureux and Thompson 2006); consequently, the high-latitude impacts of the SAM and ENSO have similar patterns during this season. The SH circulation is also marked by variability on a range of other scales (e.g., zonal wavenumber 3, Raphael 2007). However, relative to the SAM and ENSO, such variability accounts for a comparatively small fraction of the month-to-month variance in the SH atmosphere and is thus not considered here.

The influence of both the SAM and ENSO on Antarctic SIC anomalies has been documented in a number of observational and modeling studies (e.g., Simmonds and Jacka 1995; Yuan and Martinson 2000; Hall and Visbeck 2002; Kwok and Comiso 2002; Renwick 2002; Lefebvre et al. 2004; Liu et al. 2004; Holland et al. 2005; Sen Gupta and England 2006; Stammerjohn et al. 2008; Yuan and Li 2008). The positive polarity of the SAM and the cold phase of the ENSO cycle are both associated with a robust dipole pattern of increasing and decreasing SIC anomalies between the Ross/Amundsen Seas and the Antarctic Peninsula region, respectively (see Fig. 1 for the locations of the main Antarctic seas). This dipolar pattern is related to thermodynamic and dynamic forcings associated with variability in the pressure anomalies extending over the Amundsen Sea. Consistent with the atmospheric circulation, surface heat fluxes associated with warm northerly (cold southerly) winds over the Antarctic Peninsula (Ross/Amundsen Seas) promote a SIC dipole that is further reinforced by ice drift related to anomalous wind stress and attendant Ekman transport (e.g., Lefebvre et al. 2004; Liu et al. 2004; Holland et al. 2005; Lefebvre and Goosse 2005). Sea ice is also known to respond to longer-term oceanographic changes associated with the atmospheric circulation (e.g., Holland et al. 2005). The focus of this study, however, is on the shorter contemporaneous relationships between sea ice and the atmospheric circulation.

FIG. 1. Locations of the main Antarctic seas.

The anomalous SIC dipole associated with both SAM and ENSO has been well documented in the literature; however, there are several aspects of the SIC–SAM/ENSO relationship that have not been comprehensively examined. For example, evaluation of the relationships between SIC and the SAM/ENSO have generally focused on annual time scales or particular seasons of sea ice growth and decline. Given that the SH atmospheric circulation and mixed layer ocean associated with the

SAM and ENSO vary as a function of season (Ciasto and Thompson 2008), it is of interest to examine how interannual associations with SIC evolve over a full seasonal cycle. Moreover, the asymmetry of sea ice responses to positive and negative phases of the SAM/ENSO remains little explored, and further questions remain in regard to the leading patterns of SIC variability and their relation to the leading patterns of climate variability.

Beyond interannual time scales, trends in annual-mean SH SIE (and SIC) have exhibited a modest increase, but regionally, compensating areas of sea ice growth and decline emerge between the Amundsen/Bellingshausen and Ross Sea regions (e.g., Liu et al. 2004; Stammerjohn et al. 2008; Cavalieri and Parkinson 2008; Comiso and Nishio 2008). Given that a large component of high-latitude SH temperature and surface wind trends can be accounted for by trends in the SAM (Thompson and Solomon 2002), it is plausible that the SAM may also explain such trends in sea ice, particularly during the summer months. The current literature, however, is inconsistent in the degree to which sea ice trends can be attributed to trends in the SAM, ENSO, and other factors. Both Lefebvre et al. (2004) and Liu et al. (2004) suggest that there is little evidence connecting SIC trends to the SAM, whereas Goosse et al. (2009) find that their simulated trends in sea ice may reasonably be attributed to changes in the SAM-related atmospheric circulation. Several studies have also examined the connections between ozone depletion and sea ice, whereby the trend toward positive polarity of the SAM acts as the primary driving mechanism. Turner et al. (2009), for example, note consistency between trend patterns of 500-hPa geopotential height and autumn sea ice trends in the Ross Sea, surmising that the atmospheric trend pattern is in agreement with that expected from ozone depletion. Sigmond and Fyfe (2010), by contrast, find a year-round, near zonally symmetric decrease in Antarctic sea ice in response to ozone depletion. The influence of ENSO on SIC trends is also unclear, although a growing body of evidence suggests that extratropical atmospheric variability associated with the tropics has contributed to the observed SIC trends during austral spring (Schneider et al. 2012).

The goal of the present study is to provide an extensive overview of the relationships between Antarctic SIC and the SH atmospheric circulation associated with the SAM/ENSO. In doing so, we synthesize and expand upon previous work so as to 1) document the seasonal evolution of the relationships between SIC and the SAM/ENSO, 2) determine the leading patterns of SIC variability and relate these to the SAM/ENSO, 3) quantify the nonlinearity between SIC and large-scale climate variability, 4) calculate the proportion of seasonal SIC trends linearly attributable to trends in the SAM and ENSO, and 5) provide an assessment of SIC variability in high-trending regions. The rest of the paper is organized as follows. Section 2 outlines the datasets and methods. In section 3 we explore the interannual SIC variability associated with the SAM and ENSO. Section 4 examines SIC trends and their relationship to large-scale patterns of climate variability. Finally, section 5 provides a summary and the main conclusions.

2. Data and methods

The analyses of this investigation make use of monthly-mean sea ice concentration from the Met Office Hadley Centre Sea Ice and Sea Surface Temperature (HadISST) dataset (Rayner et al. 2003; http://hadobs.metoffice.com/). The data are available on a $1° \times 1°$ latitude–longitude mesh and are derived using a blended analysis of in situ and passive microwave [Scanning Multichannel Microwave Radiometer (SMMR) and Spatial Sensor Microwave/Imager (SMM/I)] retrievals that are processed using the NASA Team algorithm (NTA; Cavalieri et al. 1999). Microwave retrievals are calibrated against other satellite-derived SIC products (see Rayner et al. 2003) so as to compensate for the known negative bias in SH SIC estimates associated with NTA (Parkinson and Comiso 2008).

Monthly-mean 500-hPa geopotential heights (Z_{500}) are from the National Centers for Environmental Prediction–National Center for Atmospheric Research (NCEP–NCAR) reanalysis (Kalnay et al. 1996; Kistler et al. 2001), obtained from the NOAA/Office of Oceanic and Atmospheric Research (OAR)/Earth System Research Laboratory (ERSL) Physical Sciences Division (PSD), Boulder, Colorado (at http://www.cdc.noaa.gov/). Reanalysis data assimilates sparsely located observations (e.g., satellite, land synoptic, aircraft, and radiosonde) into physically consistent, model-generated output, interpolated onto a $2.5° \times 2.5°$ latitude–longitude grid.

Monthly SAM and ENSO indices are provided by the NOAA Climate Prediction Center (CPC) (at http://www.cpc.ncep.noaa.gov/). The SAM index is calculated by projecting monthly-mean 700-hPa (Z_{700}) height anomalies poleward of 20°S onto the leading empirical orthogonal function (EOF) of monthly Z_{700} anomalies calculated over 1979–2000; the high index polarity of the SAM corresponds to negative (positive) Z_{700} anomalies extending over Antarctica (the midlatitudes). Variability

in ENSO is characterized through the use of the cold tongue index (CTI), defined as average SST anomalies over 6°N–6°S, 180°–90°W: positive (negative) values refer to warm or El Niño (cold or La Niña) conditions. Note that the analyses involving the CTI were repeated using various other ENSO indices (e.g., Niño-3, Niño-4, Southern Oscillation index), and the results proved to be largely insensitive to the choice of index. Prior to analysis, both SAM and ENSO indices were standardized by removing the long-term mean and dividing by the long-term standard deviation; as such, regression results relate to changes for a one standard deviation positive event.

Owing to the problems associated with sparse data coverage in the SH, the analyses are restricted to the postsatellite period, 1980–2008, when data coverage is spatially continuous over Antarctica and the Southern Ocean. The choice of analysis period subsequently reduces problems associated with spurious trends in Z_{500} reanalysis products prior to the satellite era (Hines et al. 2000; Marshall 2002; Bromwich and Fogt 2004). Although all data utilized in this investigation are available to the present day, the analyses are restricted to 1980–2008 due to errors with the SSM/I data from January 2009, which results in underestimated SH SIC from this date onward.

Monthly anomalies for all datasets (SIC, Z_{500}, and climate indices) are defined as data in which the long-term climatological monthly mean has been removed. These are subsequently converted to seasonal-mean anomalies by averaging over December–February (DJF), March–May (MAM), June–August (JJA), and September–November (SON), and detrended by removing the long-term linear trend. Throughout this investigation, DJF and MAM are referred to as the warm-season months and JJA and SON as the cold-season months. Unless otherwise stated, all results are based on contemporaneous analyses of detrended, seasonal-mean anomalies.

This study makes use of correlation, regression, composite, and principal component (PC—equivalent to empirical orthogonal function) analysis. Composites are produced based on years that the index exceeds one standard deviation of the mean; the linear responses are represented using composite differences (i.e., positive − negative), and the nonlinear components expressed using composite sums (i.e., positive + negative) (e.g., Deweaver and Nigam 2002). The PCs are calculated for anomalies that are first weighted by the square root of the cosine of latitude, and the results are subsequently displayed as the unweighted seasonal-mean anomalies regressed onto the corresponding standardized PC time series. The statistical significance of the PCs is estimated as a function of the degree of separation between eigenvalues (North et al. 1982). The statistical significance of correlation coefficients, r, is measured using the two-tailed Student's t tests following Bretherton et al. (1999). A similar method is used to assess the significance of trends where the effective sample size, N_{eff}, is calculated as

$$N_{\text{eff}} = N\left(\frac{1 - r_1}{1 + r_1}\right), \tag{1}$$

where r_1 is the lag-1 autocorrelation of the *detrended* time series (Santer et al. 2000). Note that the detrended time series was used so as to prevent strong reductions in N_{eff}, and thus increasingly fewer independent samples, which would result from the incorporation of the trend into lag-1 autocorrelation values, rather than any physical season-to-season SIC variance. A threshold of statistical significance is set to 95% for all analyses.

3. Interannual SIC variability

a. Climatological features of sea ice concentration

Prior to investigating the relationships between anomalous SIC and large-scale climate variability, the key climatological features of Antarctic sea ice are reviewed. Figure 2 displays the climatological-mean SIC (contours) and the standard deviation of SIC anomalies (shading) for each season. Antarctic sea ice exhibits substantial seasonal variations in spatial extent. These variations are uninhibited by geographic constraints over the Southern Ocean and, as such, the seasonal cycle of solar insolation is clearly reflected in the seasonal cycle of ice extent. As a consequence of the large seasonal cycle, much of the ice pack is first-year ice (Comiso and Nishio 2008; Parkinson and Comiso 2008), one exception being in the Weddell Sea where the 75% isopleth persists throughout all seasons. The seasonal cycle in sea ice also exhibits strong regional dependence. For example, during the warm season months (DJF and MAM), the climatological-mean SIC in the Eastern Hemisphere is largely restricted to the vicinity of the Antarctic coast. By contrast, for much of the Western Hemisphere, the gradients in SIC largely extend farther north. During the cold season months (JJA and SON), the spatial asymmetry of the SIC climatological mean is similar to that of the warm season months but has expanded farther equatorward.

Note that the ice periphery (i.e., areas with an average SIC <75%) exhibits the highest standard deviation of SIC anomalies (Fig. 2, shading). In these regions, sea ice is more prone to the influence from passing storms, surface winds, and ocean currents. Farther poleward, the ice pack is more consolidated and thus less sensitive

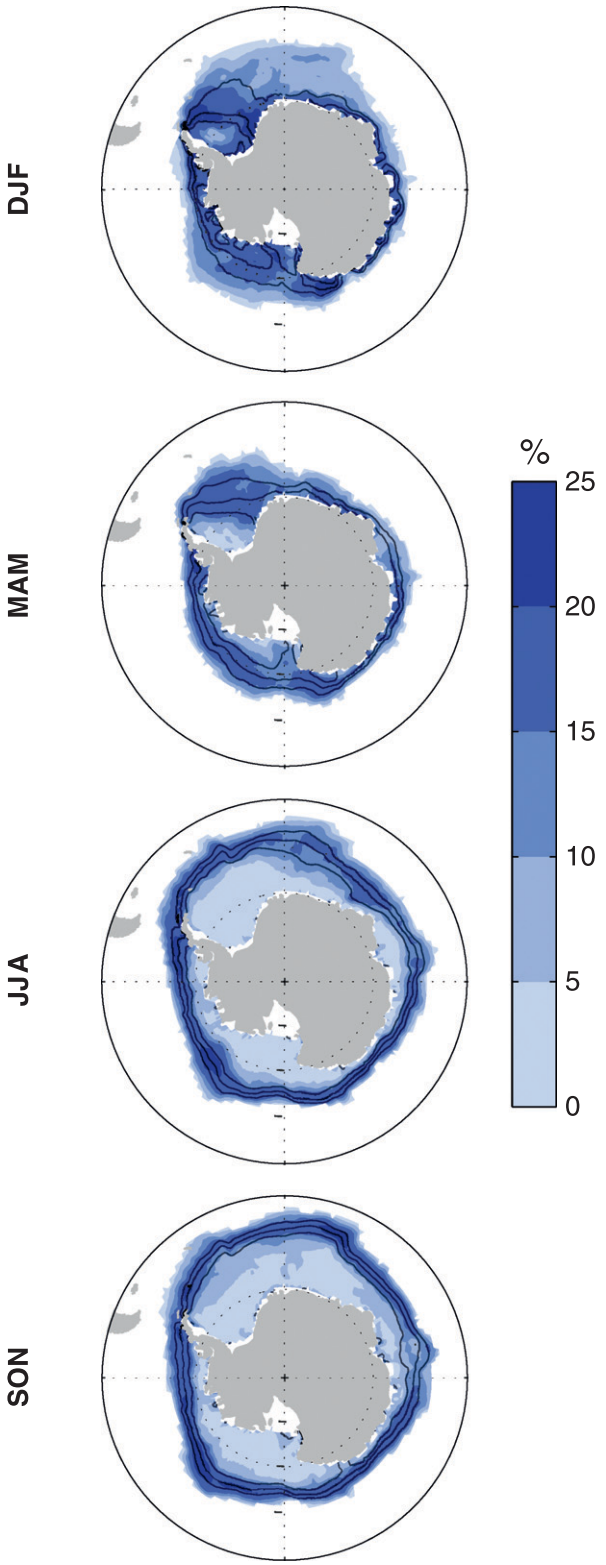

FIG. 2. Climatological mean (contours) and standard deviation (shading) of sea ice concentration (SIC) anomalies for (first row) DJF, (second row) MAM, (third row) JJA, and (fourth row) SON. Contours of the mean SIC are drawn at 25% intervals, with the 0% contour excluded.

to intraseasonal and interannual variability in the oceans and atmosphere. Two specific regions of locally enhanced variance are observed in the Bellingshausen and Ross/Amundsen Seas. Although evident in all seasons, these localized maxima display seasonal variability with regard to both structure and magnitude. SIC variability in these regions has been shown to be strongly linked to the SAM and ENSO (e.g., Liu et al. 2004; Lefebvre et al. 2004; Stammerjohn et al. 2008, and references therein) and, as such, will be the focus of subsequent analyses.

b. Relationships between sea ice concentration anomalies and patterns of large-scale climate variability

In this section, the spatial relationships between SIC and the atmospheric circulation associated with the two most prominent patterns of SH climate variability, the SAM and ENSO, are investigated. As the existing literature typically examines annual means or specific seasons of sea ice growth and decline (e.g., Liu et al. 2004; Lefebvre et al. 2004; Holland et al. 2005; Stammerjohn et al. 2008), particular focus is given to understanding the seasonal dependence of SIC–SAM/ENSO associations. Figure 3 shows Z_{500} (contours) and SIC (shading) anomalies regressed onto standardized (left panels) SAM and (right panels) ENSO indices for each season. Note that the anomalies shown in Fig. 3 correspond to the positive phase of the SAM and the warm phase of the ENSO cycle. The atmospheric structures of both the SAM and the high-latitude response to ENSO are comparable at all levels of the troposphere (Karoly 1989; Thompson and Wallace 2000). As such, the surface circulation, and thus surface winds, can be inferred from Z_{500} heights when assuming geostrophy.

The results in the left column of Fig. 3 illustrate that seasonal variations in the nonannular component of the SAM (i.e., the negative height anomalies extending over the Amundsen Sea) give rise to considerable seasonal variations in the structure and magnitude of the underlying SIC dipole. Although considerable seasonal differences are evident, similar patterns emerge between DJF and MAM (i.e., the warm season months) and also between JJA and SON (i.e., the cold season months). During the warm season months, the positive phase of the SAM is associated with negative (positive) SIC anomalies in the Bellingshausen/western Weddell (Ross/Amundsen) Seas. Such SIC anomalies are consistent with the physical impacts of negative height anomalies over the Amundsen Sea: warm (cold) air advection and southward (northward) ice drift and Ekman transport in the vicinity of the Antarctic Peninsula (Ross Sea) (e.g., Lefebvre et al. 2004; Liu et al. 2004; Holland et al. 2005; Lefebvre and Goosse 2005, and references

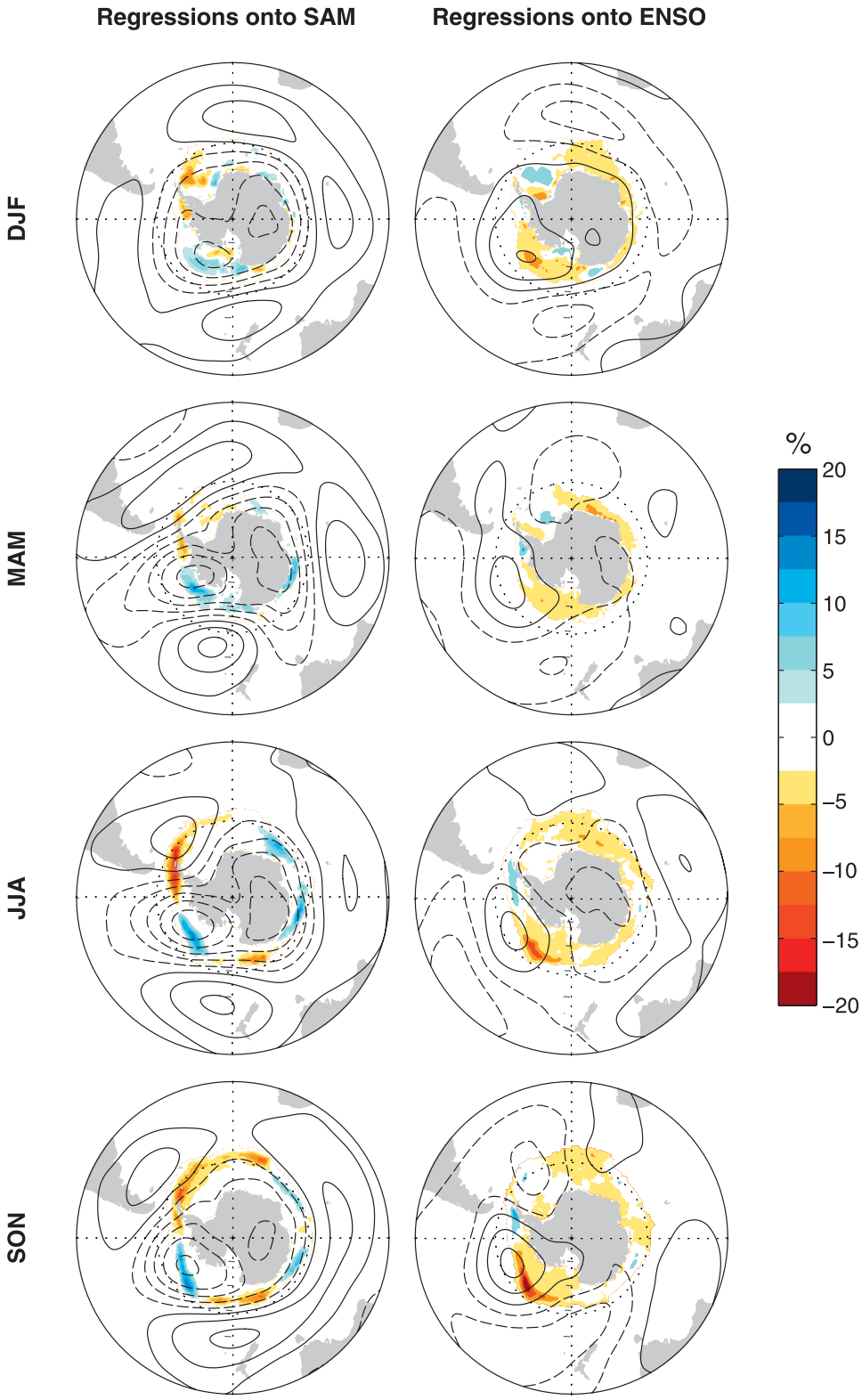

FIG. 3. Seasonal-mean Z_{500} (contours) and SIC (shading) anomalies regressed onto standardized (left) SAM and (right) ENSO indices for (first row) DJF, (second row) MAM, (third row) JJA, and (fourth row) SON. Positive (negative) contours are denoted by solid (dashed) lines and are drawn at intervals of 10 m (−15, −5, 5, 15 m…).

therein). However, during the cold season months, shifts in the location of the negative height anomalies over the Amundsen Sea result in an eastward migration of the SIC dipole such that negative (positive) SIC anomalies now extend across the Bellingshausen/Weddell (Amundsen/western Ross) Seas (Fig. 3). The cold season SIC dipole is also observed to be considerably stronger in magnitude than its warm season counterpart, a difference that may be related to the enhancement of air–sea heat fluxes during the cold season months (Ciasto and Thompson 2008). These anomalous heat fluxes will, in turn, enhance the perturbations of an SST field already near the freezing point, and thus already primed for sea ice growth. In the warm season months, by contrast, much stronger heat flux anomalies are necessary to drive variability in the sea ice field. The analyses in Fig. 3 were also repeated at one-month lag (e.g., JFM SIC regressed onto the DJF SAM) and qualitatively similar results were obtained (not shown).

Similar to the SAM, the influence of the SH atmospheric circulation associated with ENSO on Antarctic SIC anomalies varies as a function of season. Strong similarities exist between the atmospheric signatures of the SAM and ENSO during DJF (Karoly 1989; L'Heureux and Thompson 2006), and these similarities are thus reflected in the associated anomalous SIC field (Fig. 3, top-right panel; note that the positive polarity of the SAM is linked to the cold phase of ENSO, whereas the results in Fig. 3 display those for the warm phase of ENSO). ENSO is associated with weak SIC anomalies during the warm season months. The sea ice variability fails to take significant form, as evidenced by the pattern of relatively weak and geographically diffuse anomalies. The limited magnitude of warm season SIC anomalies is likely due to a weaker pattern of atmospheric circulation anomalies that are insufficient to substantially perturb the sea ice field. In JJA and SON, however, a distinct SIC dipole pattern emerges in association with ENSO, in accordance with the stronger relationship between SIC anomalies and atmospheric circulation anomalies during this time. Consistent with enhanced Z_{500} anomalies, the magnitude of the SIC dipole also peaks during SON when the tropical–extratropical connection is enhanced (Jin and Kirtman 2009). Nevertheless, during all seasons, the ENSO-related SIC anomalies are substantially weaker and more geographically confined than the SAM equivalents. These findings are consistent with Stammerjohn et al. (2008), who also note that during DJF and MAM the connection between ENSO and sea ice advance/retreat is weaker compared to the SAM. By contrast, other studies often find a comparable, if not stronger, relationship between SIC and ENSO (e.g., Liu et al. 2004; Yuan and Li 2008). These previous studies, however, are based on annual statistics, suggesting that the season during which ENSO influences sea ice variability is important. Note that these analyses were also repeated using several ENSO indices, and the results remained qualitatively similar.

The authors now examine the extent to which the leading patterns of SIC variability relate to variability in the SAM and ENSO using EOF/PC analysis. To our knowledge, this has previously only been examined using model output (Holland et al. 2005). Figure 4 shows seasonal-mean SIC (shading) and Z_{500} (contours) anomalies regressed onto the standardized (left panels) first and (right panels) second PC time series of SIC (PC_{SIC1} and PC_{SIC2}, respectively). According to the criterion outlined in North et al. (1982), PC_{SIC1} and PC_{SIC2} are well separated from each other and from the associated third PCs; the percentages of variance explained by each pattern are given in Fig. 4.

In all seasons, the leading patterns of SIC variability exhibit the largest amplitudes in regions that coincide with the largest standard deviation (Fig. 2), but the extent to which the SIC patterns are related to the SAM and ENSO varies between seasons. During the warm-season months, the connection between the leading patterns of SIC variability and the SAM and ENSO is somewhat ambiguous. In DJF, the pattern of SIC anomalies associated with PC_{SIC1} projects onto those associated with both the positive polarity of the SAM and the cold phase of ENSO. However, the associated Z_{500} anomalies only bear a slight resemblance to a weakened SAM-like structure. Furthermore, PC_{SIC1} is significantly correlated with ENSO ($r = 0.39$), but the correlations with the SAM ($r = 0.35$) fail to meet the 95% significance level (Table 1). In MAM a significant correlation is also observed between the SAM and PC_{SIC2} and, although the pattern of Z_{500} anomalies projects onto the SAM, this connection is modest.

In the cold season months, JJA and SON, the relationships between the leading patterns of SIC variability and the SAM and ENSO are more coherent and distinct. Figure 4 reveals that the dominant patterns of cold season SIC variability (PC_{SIC1}) project onto those associated with the SAM (cf. Figs. 3 and 4, bottom two left panels); in JJA/SON, correlations with PC_{SIC1} and the SAM are statistically significant at the 95% level and are stronger than those during DJF/MAM (Table 1). Although significantly related to the SAM, the patterns of Z_{500} anomalies associated with PC_{SIC1} appear slightly more wavelike, particularly in JJA. A comparison of the observed and model-derived (Holland et al. 2005) leading patterns of SIC variability in JJA and JJAS, respectively, reveals considerable consistency in the

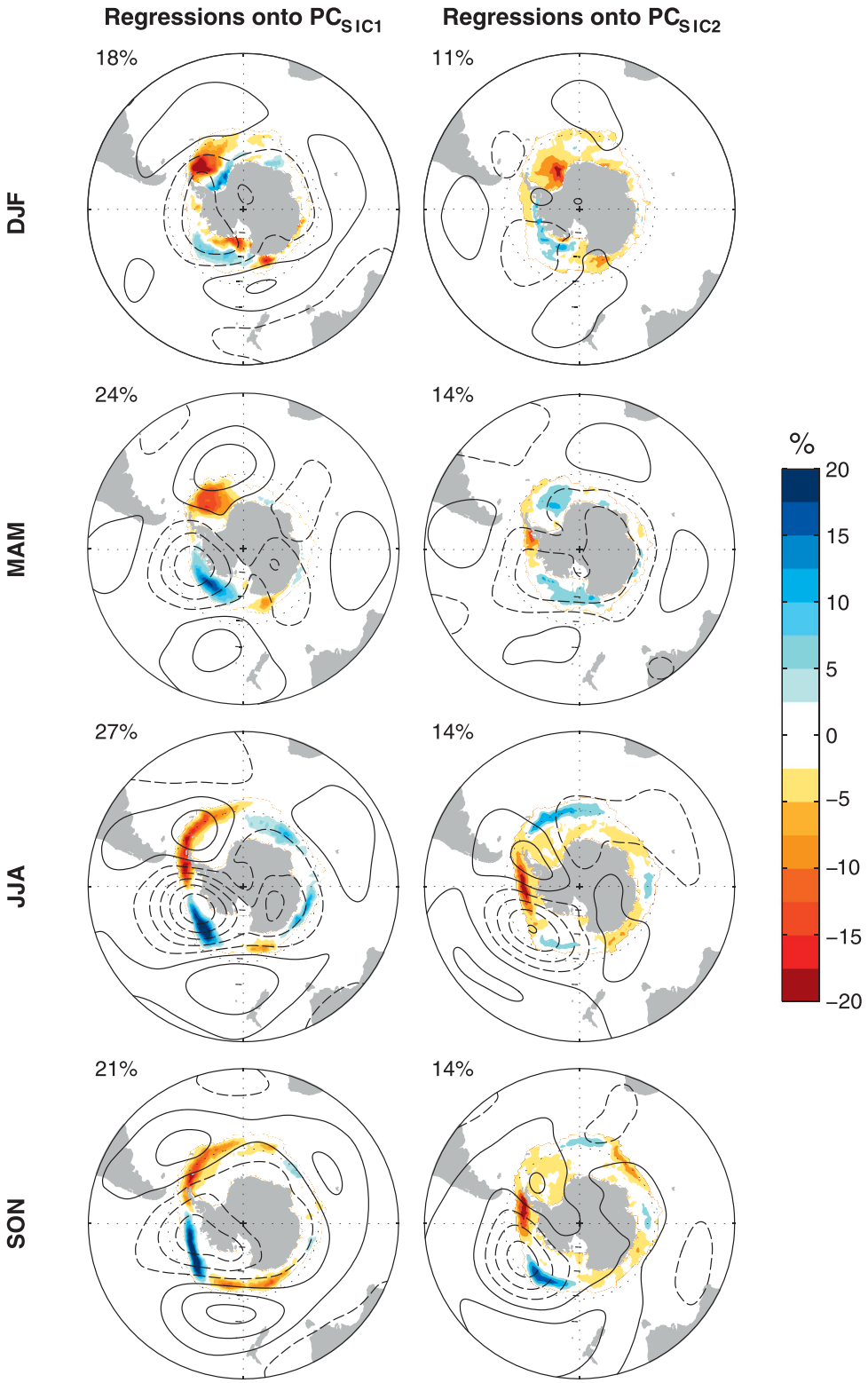

FIG. 4. As in Fig. 3 but for Z_{500} (contours) and SIC (shading) anomalies regressed onto standardized (left) PC_{SIC1} and (right) PC_{SIC2}. The value (top-left above each panel) describes the percentage variance explained by each mode.

TABLE 1. Correlation coefficients between the first two principal component time series of Southern Hemisphere seasonal sea ice concentration and the SAM and cold tongue ENSO index. Boldface values indicate results statistically significant at the 95% level as determined by two-tailed t tests.

	SAM		ENSO	
	$r(PC_{SIC1})$	$r(PC_{SIC2})$	$r(PC_{SIC1})$	$r(PC_{SIC2})$
DJF	0.35	0.03	**−0.39**	−0.26
MAM	0.35	**0.45**	−0.28	−0.17
JJA	**0.63**	0.17	−0.27	−0.27
SON	**0.58**	0.14	−0.28	**−0.60**

spatial patterns of SIC anomalies. Interestingly, Holland et al. (2005) find a substantially weaker correlation with the SAM index (maximum $r = 0.35$ at 1-yr lag) relative to that presented here ($r = 0.63$, Table 1). This weaker association may, in part, be due to the greater zonal symmetry of the model-derived SAM compared to the observations.

Although the regression and PC analyses shown in Figs. 3–4 highlight key features associated with the SAM and ENSO, these linear statistical techniques assume that positive and negative events have an equal and opposite response. However, it is known that the SST anomalies associated with El Niño and La Niña events have a nonlinear component (e.g., Deweaver and Nigam 2002) that may potentially affect the teleconnections to, and thus impacts on, the SH extratropics. To determine the nonlinearity in the SIC and Z_{500} fields, composite analyses are performed based on those years when the SAM and cold tongue indices exceed one standard deviation of the mean. The linear components of the SIC–SAM/ENSO relationship are expressed using composite differences, that is, positive − negative. The nonlinear components, or the departure from symmetry, are calculated using composite sums, that is, positive + negative (e.g., Deweaver and Nigam 2002). Note that although the composites are derived using relatively few samples, the subsequent results are not sensitive to small changes in the combination of positive and negative events used. Figures 5 and 6 display the composite differences (left panels) and composite sums (right panels) for the SAM and ENSO, respectively. As in previous figures, shading (contours) represents SIC (Z_{500}); note, however, that the scaling for both variables has changed.

Consistent with the regression analysis, composite difference maps of SIC and Z_{500} anomalies (i.e., the linear components) reaffirm that seasonality in the nonannular component of the SAM gives rise to a seasonally varying SIC dipole that peaks during the cold season months (cf. Figs. 3 and 5, left panels). However, maps of the composite sums suggest an asymmetry in the atmospheric circulation anomalies between positive and negative phases of the SAM (Fig. 5, right panels, contours). These nonlinearities are largely centered over the Amundsen Sea, and consequently nonlinearity also arises in the SIC field. Nevertheless, the magnitudes of the nonlinear components are observed to be substantially smaller than those of the linear components. As such, the relationship between the SAM and SIC can be approximated as linear.

Similar to the SAM, the ENSO composite difference maps also project onto the associated regression maps (cf. right panels in Fig. 3 with left panels in Fig. 6) and are statistically significant at the 95% confidence level (Fig. 6, left panel). In contrast to the SAM, however, the ENSO-related composite sums highlight substantial differences between El Niño and La Niña events, with magnitudes often exceeding those of the composite differences. Such substantial nonlinearities indicate a considerable phase dependence regarding the positioning of the ENSO-induced SH atmospheric wave train, particularly in SON when the tropical–extratropical connection is strongest (Fig. 7). Relative to El Niño, the La Niña wave train signature in Z_{500} anomalies has shifted such that anomalies are observed farther west. These shifts in the location of extratropical Z_{500} anomalies between phases of the ENSO cycle accordingly explain the nonlinearities evident in SIC anomalies (Fig. 6, right panels) and, thus, emphasize the need to consider ENSO associations with sea ice by phase. Note that a similar analysis for positive and negative composites of the SAM was not shown due to the more linear nature of its signature in the Z_{500} and sea ice fields (Fig. 5).

Figures 3–7 have examined how interannual SIC variability associated with the SAM and ENSO varies as a function of season. In the majority of cases, a seasonally varying sea ice dipole emerges due to the physical impacts of the anomalous atmospheric circulation related to the SAM and ENSO. A seasonal examination of SIC–SAM/ENSO relationships reveals that Antarctic sea ice anomalies exhibit strongest linkages to the SAM and ENSO during the cold season months, JJA and SON, with considerably weaker SIC–atmosphere relationships emerging during DJF and MAM. Moreover, it was shown that ENSO associations with sea ice exhibit a substantial level of nonlinearity (Figs. 6 and 7), highlighting the importance of considering both the season and the phase of the ENSO cycle when diagnosing its relationship with sea ice.

4. Trends in sea ice concentration over 1980–2008

a. Relationships between trends in sea ice concentration and the SAM and ENSO

As the SAM and ENSO have strong interannual associations with sea ice (as highlighted in the preceding

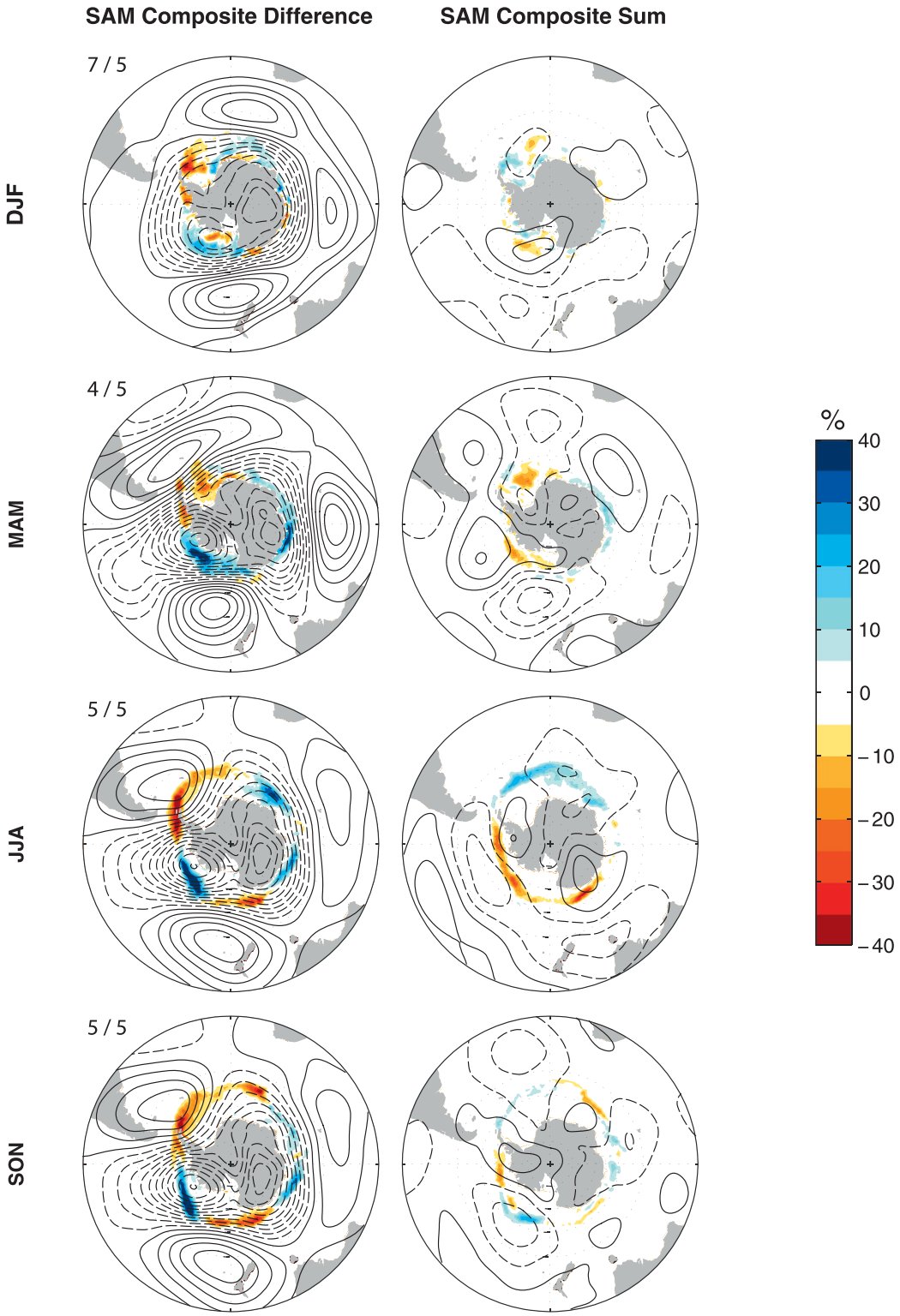

FIG. 5. (left) Composite differences and (right) composite sums of seasonal-mean Z_{500} (contours) and SIC (shading) anomalies averaged over seasons wherein the SAM index exceeds one standard deviation. Positive (negative) contours are denoted by solid (dashed) lines and are drawn at intervals of 15 m (−22.5, −7.5, 7.5, 22.5 m…). The values (top-left above the composite differences) indicate the number of positive/negative seasons, respectively, that were used to create the composite.

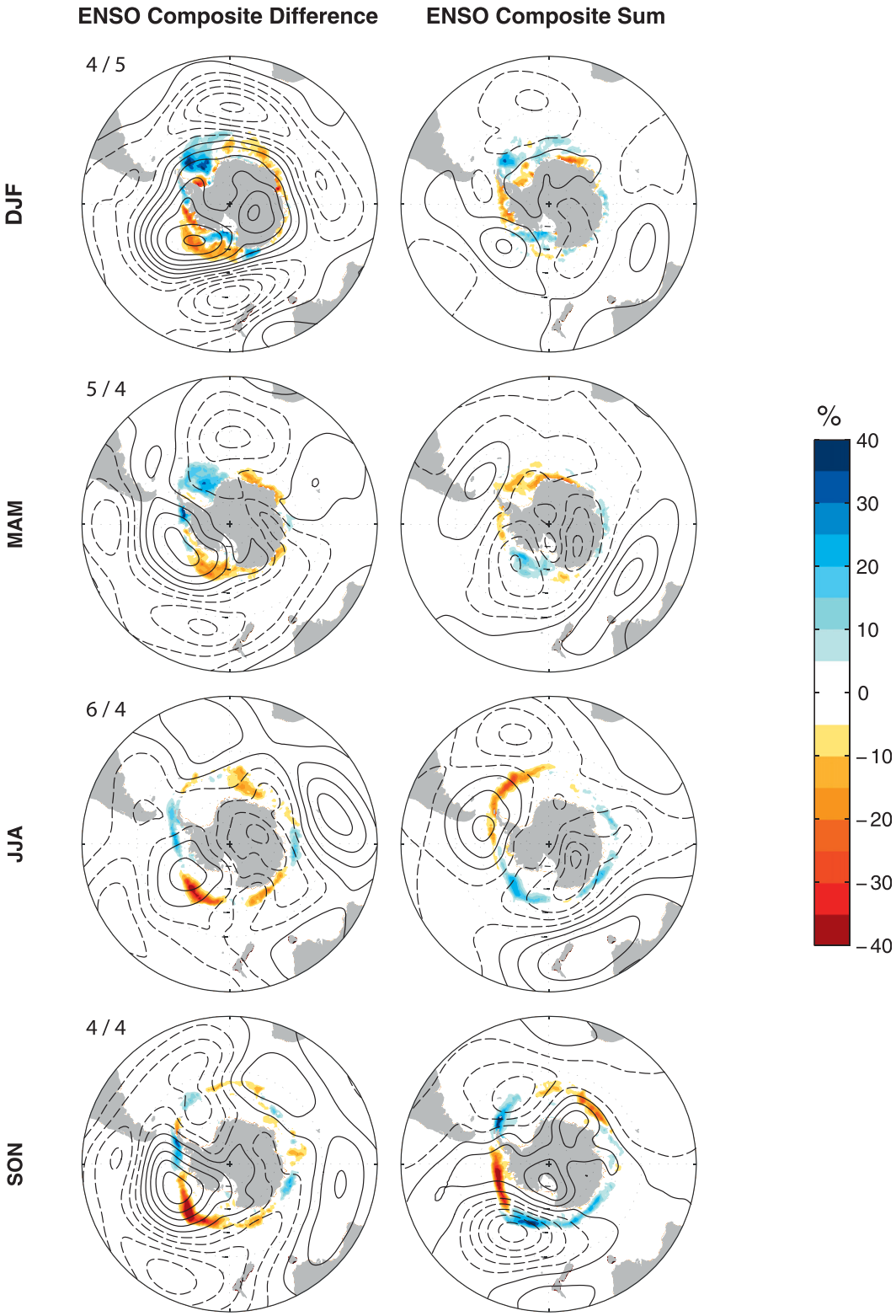

FIG. 6. As in Fig. 5 but for (left) composite differences and (right) composite sums based on seasons wherein the cold tongue ENSO index exceeds one standard deviation.

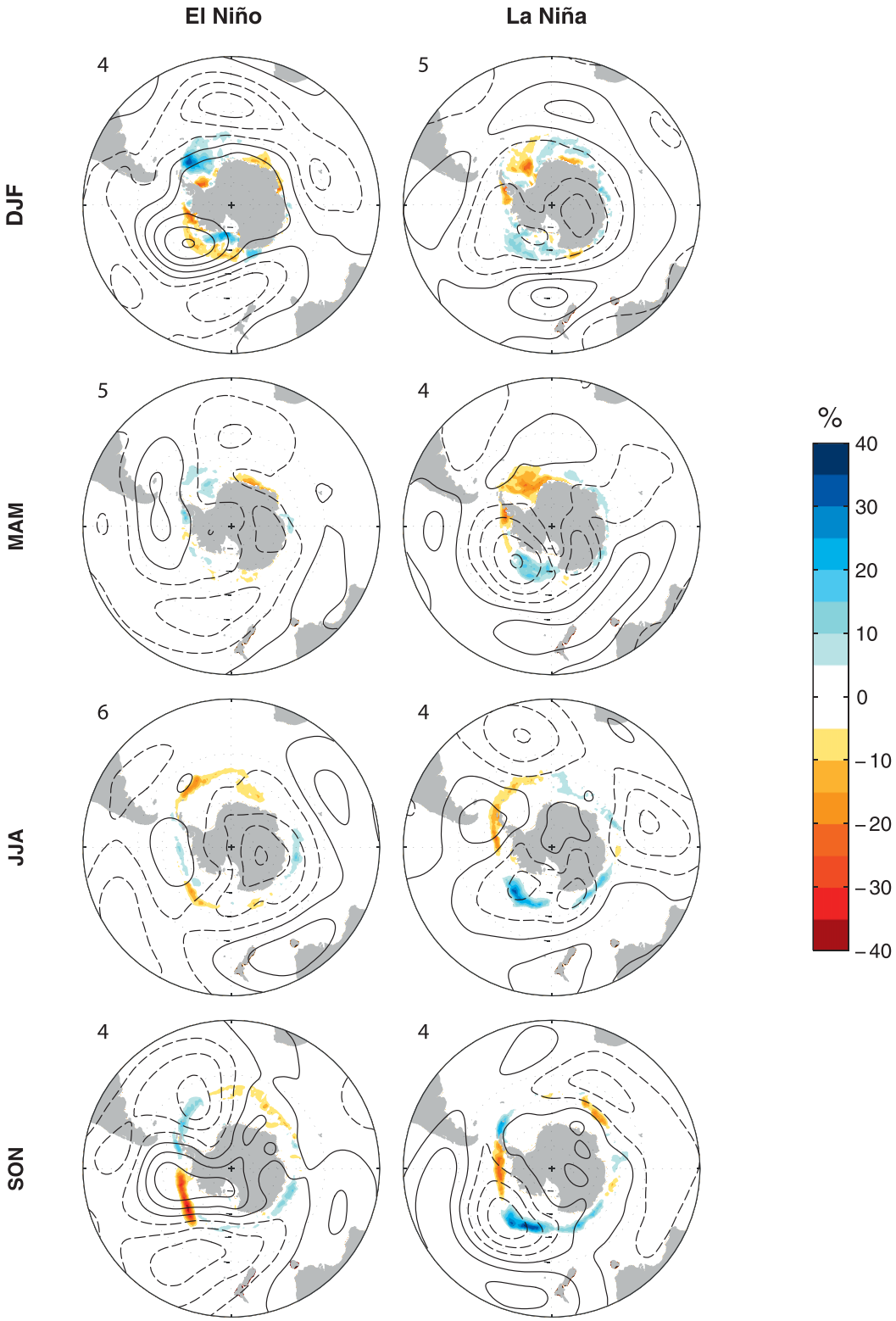

FIG. 7. (left) El Niño and (right) La Niña composites of seasonal-mean Z_{500} (contours) and SIC (shading) anomalies averaged over seasons wherein the cold tongue ENSO index exceeds one standard deviation. Positive (negative) contours are denoted by solid (dashed) lines drawn at intervals of 15 m (−22.5, −7.5, 7.5, 22.5 m. . .). The value (top-left above each panel) indicates the number of seasons used to create the composite.

section), it is of interest to examine the extent to which trends in SIC can also be attributed to trends in the SAM and ENSO. Moreover, given that high-latitude SH temperature and surface wind trends are strongly coupled with trends in the SAM (Thompson and Solomon 2002; Marshall 2007), there is a reasonable expectation that summertime SIC trends may also be driven by the SAM.

Figure 8 displays the total observed SIC trends over 1980–2008 (note that the color scales have changed from previous figures and that warm colors denote decreasing SIC and vice versa). In all seasons, the SIC trends are characterized by positive SIC anomalies in the Ross Sea and negative SIC anomalies in the Bellingshausen Sea, consistent with previous studies of annual and seasonal SIC, SIE, and sea ice advance/retreat (Liu et al. 2004; Cavalieri and Parkinson 2008; Comiso and Nishio 2008; Stammerjohn et al. 2008). Figure 8 also demonstrates considerable seasonal variability in the structure and magnitude of SIC trends, with noticeable differences observed between the warm, DJF and MAM, and cold, JJA and SON, season months. In the warm season months, SIC trends are centered over the Bellingshausen and western Ross (150°E–180°) Seas, and the respective decreases and increases peak at magnitudes of ~40%–50% over the 29-yr period. During the cold season months, by contrast, negative SIC trends extend eastward from the eastern Ross Sea to the Amundsen, Bellingshausen, and Weddell Seas, with magnitudes peaking at 25%–35% in the Bellingshausen Sea. In the Ross Sea region positive SIC trends of >40% are maintained but are shifted northward and extended zonally relative to the warm seasons, consistent with the seasonal cycle of sea ice (Fig. 2).

The authors now quantify the proportion of contemporary SIC trends that are linearly congruent with the two leading patterns of SH climate variability. The subsequent analysis, however, focuses specifically on those changes related to the SAM during austral summer because 1) the time series of tropical SST indices have exhibited no significant trends during any season (e.g., Nicholls 2008) and 2) the trends in the SAM index are most pronounced in DJF (Marshall 2007). The proportion of SIC and Z_{500} trends that are linearly congruent with the SAM during DJF were calculated by regressing seasonal-mean SIC and Z_{500} anomalies onto the detrended SAM index, and then multiplying the resulting regression coefficients by the trend in the SAM. The residual (i.e., the component of the trends that cannot be linearly attributed to the SAM) was defined as the linearly congruent components subtracted from the original trends. Figure 9 displays the total observed DJF trends, the fraction of trends linearly congruent with the DJF SAM, and the residual trends after

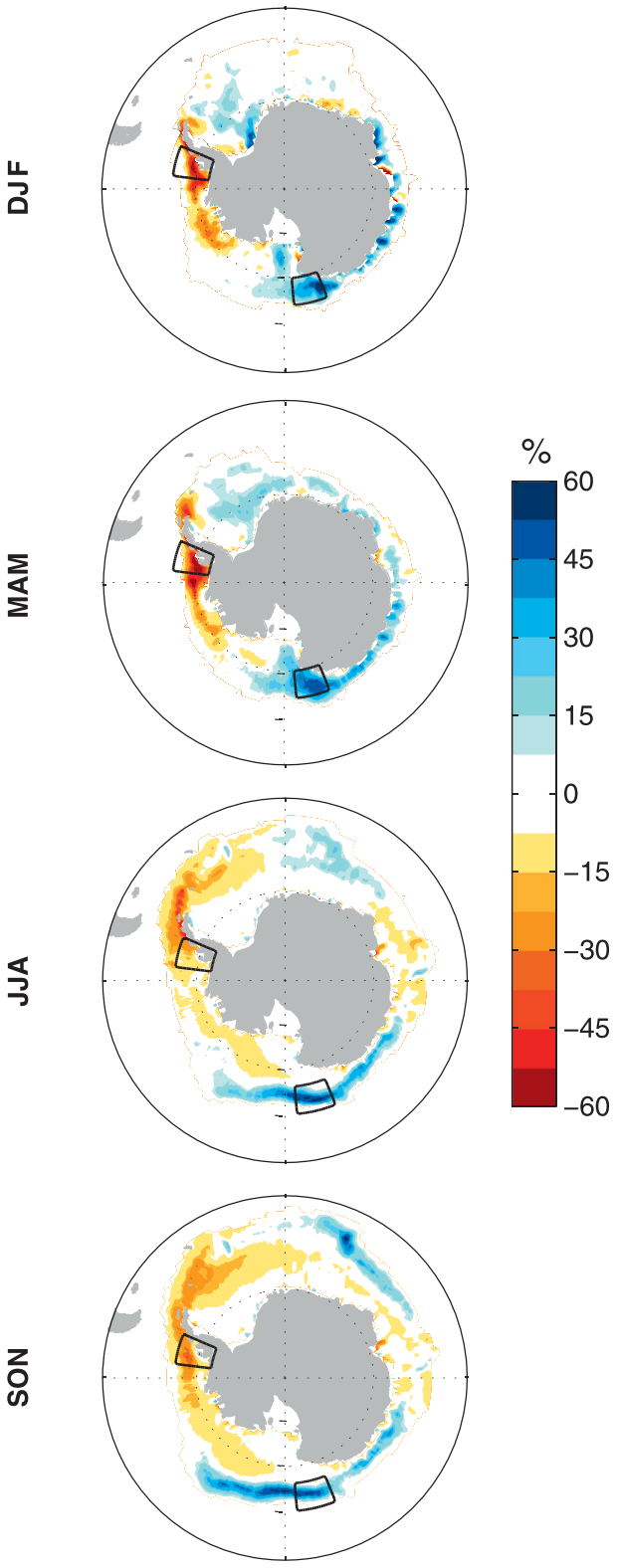

FIG. 8. Linear trends in seasonal-mean SIC calculated over 1980–2008 for (first row) DJF, (second row) MAM, (third row) JJA, and (fourth row) SON. Black boxes define the areas used to calculate regional sea ice time series (Fig. 10).

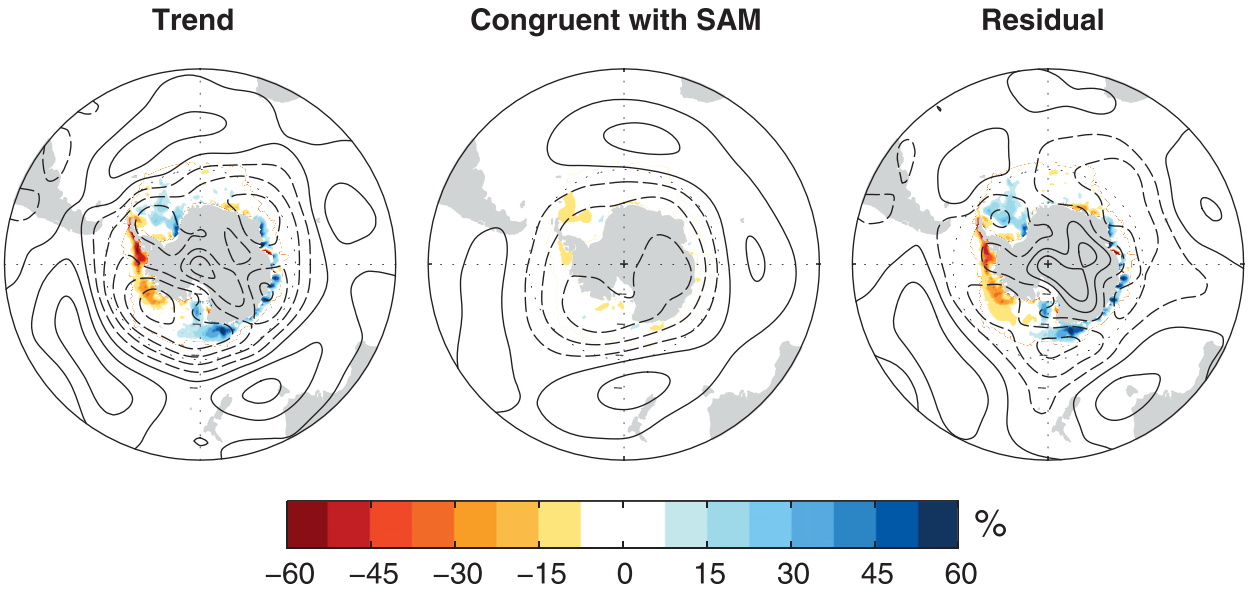

FIG. 9. (left) DJF Z_{500} (contours) and SIC (shading) trends calculated over 1980–2008, (middle) the proportion of trends congruent with DJF SAM, and (right) the residual trends after removing the effects of the DJF SAM. Positive (negative) contours are denoted by solid (dashed) lines drawn at intervals of 15 m (−22.5, −7.5, 7.5, 22.5 m. . .).

removing the effects of the DJF SAM, for Z_{500} (contours) and SIC (shading); note that the contour intervals of Z_{500} anomalies have altered from previous figures.

Consistent with the observed trend toward the positive polarity of the SAM, the spatial pattern of Z_{500} trends shows a clear annular structure. In agreement with Thompson and Solomon (2002), a large fraction of these trends is congruent with the SAM (Fig. 9, contours). By contrast, the proportion of DJF SIC trends linearly attributable to the SAM is negligible; at the most, congruencies peak at <15% within localized regions (middle panel in Fig. 9, shading). Consequently, the residual displays magnitudes comparable to the SIC trends (cf. left and right panels in Fig. 9). Given that the dipolar patterns of the SIC trends do not project onto the patterns of interannual variability associated with the SAM (cf. DJF panels of Figs. 3 and 8, shading), the limited connection between summertime SIC and SAM trends is not necessarily unexpected. The congruency analyses were repeated for all seasons at both contemporaneous and multiple lags, for both SAM and ENSO. In all cases, trends in the two leading patterns of SH climate variability were unable to account for a significant component of the 1980–2008 SIC trends (not shown). Such conclusions are consistent with previous studies that have 1) examined the congruencies between SIC and the SAM and ENSO at annual time scales (Liu et al. 2004), 2) calculated the congruency of SIC trends to a regional SAM index for SON only (Schneider et al. 2012), and 3) inferred congruency via comparisons of the patterns of SIC–SAM regressions to SIC trends (Lefebvre et al. 2004). Schneider et al. (2012), however, find that higher order PCs of regional extratropical geopotential height anomalies associated with the tropics can account for a larger fraction of SIC trends but such PCs are not examined here.

b. *Sea ice concentration variability in high trending regions*

As demonstrated by Fig. 8, both the Bellingshausen and Ross Sea regions have exhibited strong seasonal SIC trends, motivating further investigation of SIC variability in these locations. Sea ice time series were created for this purpose by averaging seasonal-mean SIC anomalies over two regions. The Bellingshausen time series is calculated by averaging over 65.5°–72.5°S, 65.5°–82.5°W and the Ross time series over 64.5°–69.5°S, 158.5°–174.5°E in DJF and MAM but 60.5°–65.5°S, 158.5°–174.5°E in JJA and SON to coincide with the regions of maximum trends (for location, see boxes in Fig. 8). By definition, these regions were chosen to encompass the strongest SIC trends, but we note that the areas of maximum trends are not precisely incorporated in every season (e.g., the Ross Sea during DJF and the Bellingshausen Sea during JJA). The subsequent results, however, were largely insensitive to modest zonal and meridional changes to the box boundaries. These regions were not defined with the purpose of capturing

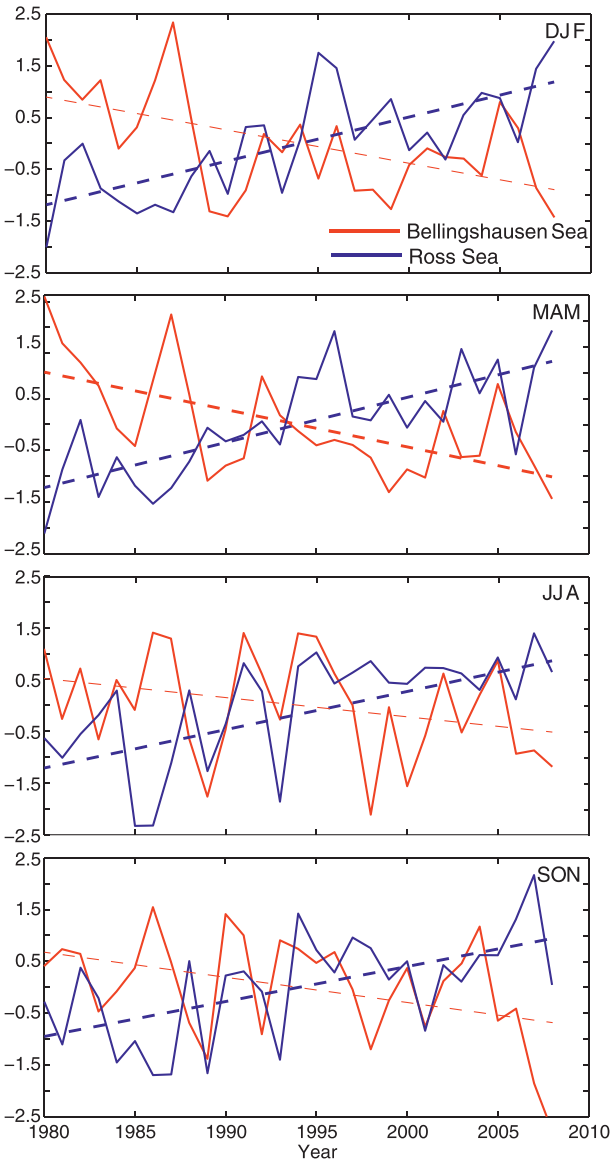

FIG. 10. Standardized seasonal-mean Bellingshausen Sea (red) and Ross Sea (blue) sea ice time series for (first row) DJF, (second row) MAM, (third row) JJA, and (fourth row) SON. Dashed lines represent the line of best fit with thick lines denoting statistically significant trends, as quantified in Table 2. Time series correspond to the average SIC over the region defined by black boxes shown in Fig. 8.

SIC variability associated with the SAM or ENSO (i.e., the SIC dipole observed in Figs. 3–6) but some overlap is evident, particularly during the cold season months.

Figure 10 shows the standardized sea ice time series for the Bellingshausen (red) and Ross (blue) Sea regions. The Bellingshausen time series is observed to experience negative trends over 1980–2008 in all seasons. However, when evaluating the significance of these trends [using N_{eff} from Eq. (1)], it becomes apparent that statistically

TABLE 2. Seasonal linear trends in the Bellingshausen and Ross Sea time series calculated over 1980–2008, and correlation coefficients between the Bellingshausen Sea and Ross Sea time series, and the SAM and cold tongue ENSO index. Boldface values indicate results that are statistically significant at the 95% level as determined by two-tailed t tests.

	Bellingshausen Sea			Ross Sea		
	Trend	r(SAM)	r(ENSO)	Trend	r(SAM)	r(ENSO)
DJF	−1.86	−0.34	0.27	**2.46**	0.31	0.07
MAM	**−2.10**	−0.35	**0.45**	**2.53**	0.29	−0.19
JJA	−1.07	**−0.50**	0.35	**2.15**	**−0.46**	−0.04
SON	−1.41	−0.24	**0.39**	**1.96**	**−0.50**	0.07

significant trends occur during MAM only (Table 2). By contrast, the Ross Sea time series exhibits statistically significant positive trends in all seasons (Table 2). Correlations between the Ross and Bellingshausen time series (not shown) fail to exceed the 95% confidence level in any season, indicating that separate processes may be driving SIC variability in these two high trending regions.

The regressions of Z_{500} and SIC anomalies onto the Bellingshausen and Ross Sea time series (Fig. 11, left and right panels, respectively) illustrates that warm season sea ice variability exhibits a limited association with the overlying atmospheric circulation anomalies in both locations. This notion is further supported by significant correlations only being evident between the Bellingshausen time series and ENSO during MAM (Table 2). Such conclusions are consistent with earlier results that also note a weakened warm season connection between SIC variability and the SAM and ENSO on interannual (Figs. 3–7) and longer (Fig. 9) time scales.

During the cold season months, by contrast, SIC variability in the Ross and Bellingshausen Sea regions exhibits a stronger association with the atmospheric circulation anomalies (Fig. 11), consistent with previous findings presented here (Figs. 3–7). Of particular interest is the differing atmospheric circulation patterns that emerge between the two regions (Fig. 11, bottom two panels), highlighting that separate mechanisms may be forcing SIC variability in the Bellingshausen and Ross Sea regions. The Bellingshausen time series, for example, is found to be significantly related to the SAM in JJA (Fig. 11, Table 2) but is associated with a much more wavelike pattern of Z_{500} anomalies (cf. bottom two panels, Figs. 3 and 11). In SON the Bellingshausen time series is related to a similar wavelike pattern, but is significantly correlated with ENSO during this season (Table 2). In the Ross Sea region, however, the structure of height anomalies in both JJA and SON projects onto the conventional zonally symmetric signature of the SAM (Fig. 11), and significant

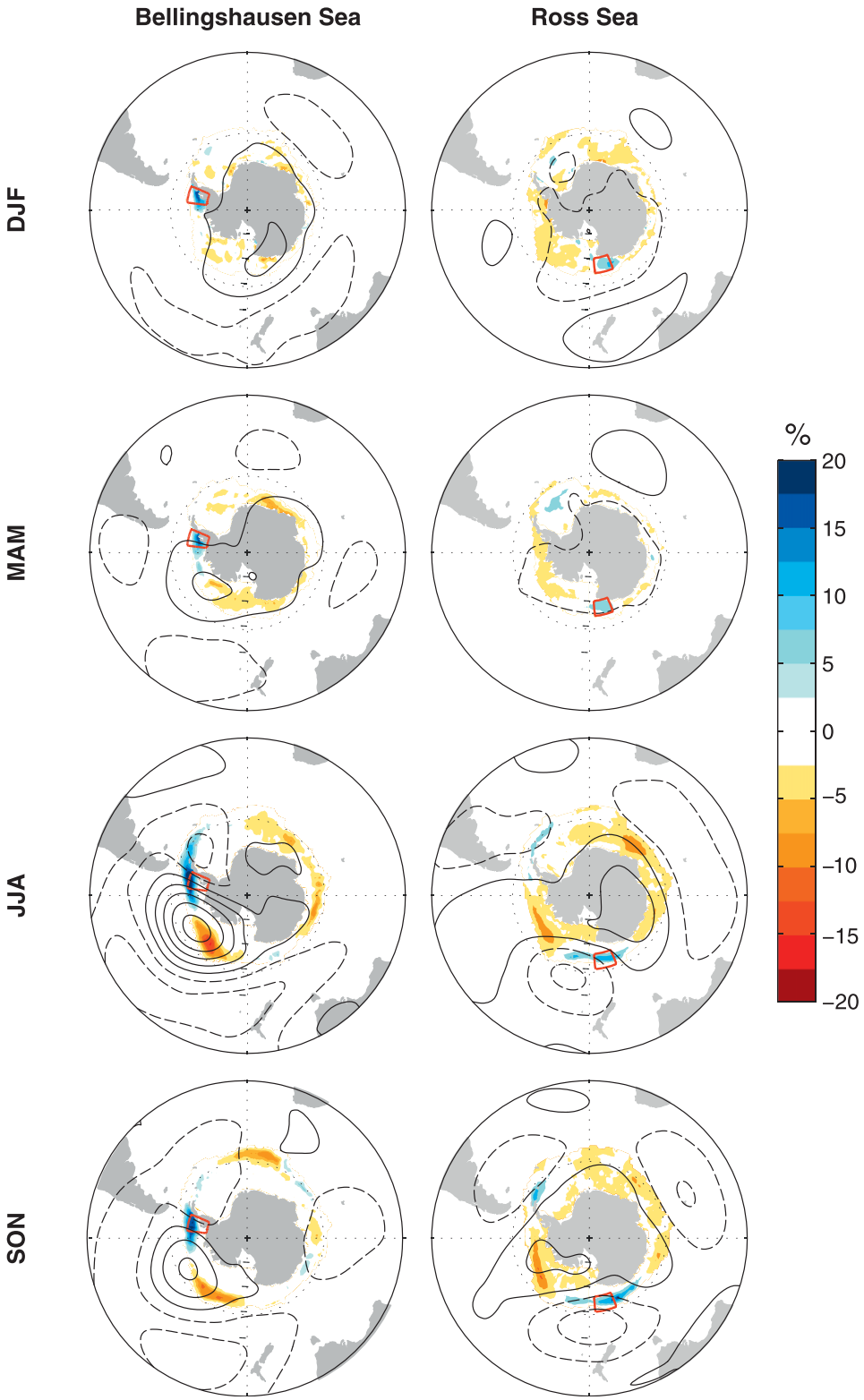

FIG. 11. As in Fig. 3 but for Z_{500} (contours) and SIC (shading) anomalies regressed onto standardized sea ice time series from the (left) Bellingshausen and (right) Ross Sea regions. Red squares define the spatial limit of the area used to create the sea ice time series and correspond to the black boxes of Fig. 8. Note that the Ross Sea box moves equatorward during JJA and SON.

correlations to the SAM are observed in both seasons (Table 2). This SAM-related pattern of variability is likely because the box defining the Ross Sea time series coincides with a region of positive SIC anomalies associated with the SAM.

5. Summary and conclusions

The results presented here provide an extensive overview of the observed relationships between seasonal Antarctic SIC and the atmospheric circulation associated with the two leading patterns of SH climate variability, the SAM and ENSO. The key findings from this study are as follows.

1) *The structure of Antarctic SIC anomalies associated with the SAM and ENSO exhibit considerable seasonal variations.*
   Consistent with previous studies, both the SAM and ENSO are found to be associated with a dipolar pattern of SIC anomalies in the vicinity of the Antarctic Peninsula and the Ross/Amundsen Sea. Here we extend previous studies by examining results for all seasons. In doing so, it has become evident that the structure and magnitude of the SAM/ENSO-related sea ice dipole varies strongly as a function of season, strengthening from the warm to the cold season months. Such seasonal variations are consistent with the seasonality of the overlying atmospheric circulation anomalies (Figs. 3–7). A comparison of the SIC anomalies associated with the leading patterns of climate variability reveals that ENSO-related SIC variability tends to be weaker and more diffuse than SAM-related SIC variability (Fig. 3). Nevertheless, during DJF the patterns of sea ice anomalies associated with the SAM and ENSO project strongly onto each other, highlighting the need to consider the seasonal SAM/ENSO relationship when evaluating ENSO associations with sea ice.
2) *Antarctic sea ice variability exhibits an enhanced connectivity to the atmospheric circulation associated with the SAM and ENSO during the cold season months.*
   As previous studies typically evaluate SIC–SAM/ENSO relationships on annual time scales or a select few seasons, the relative connectivity of SIC variability to the SAM and ENSO has been little considered. Through analyzing all four seasons, however, it has become apparent that both the SAM and ENSO exhibit the strongest linkages to Antarctic sea ice during the cold season months. While the magnitude of atmospheric circulation anomalies associated with the SAM and ENSO is roughly comparable during all seasons, the strength of the underlying SIC anomalies is found to be substantially stronger during JJA and SON (Figs. 3 and 5–7). It is hypothesized that such enhanced connections may be related to the ability of anomalous heat fluxes to perturb the climatological-mean SST field to impact sea ice. Furthermore, EOF/PC analyses reveal that the leading patterns of warm season SIC variability are only weakly associated with any large-scale pattern of climate variability, whereas more dominant linkages to SAM/ENSO emerge during JJA and SON (Table 1, Fig. 4). Similarly, only JJA and SON SIC variability in the Bellingshausen and Ross Seas are strongly linked to large-scale patterns of atmospheric circulation during the cold seasons (Fig. 11, Table 2). Consequently, SIC variability during the warm seasons may be impacted by other factors that are not considered here.
3) *The impacts of the high-latitude ENSO teleconnection to sea ice are highly phase dependent.*
   Past considerations of SIC–SAM/ENSO relationships have primarily focused on linear statistical techniques, with little discussion of any nonlinear associations. While the phase dependence has been examined through the use of composite analysis (e.g., Kwok and Comiso 2002; Stammerjohn et al. 2008), to our knowledge the nonlinear components (expressed using composite sums) have not hitherto been presented. We therefore further previous studies by examining the asymmetry in positive and negative SAM/ENSO events and their impact on seasonal sea ice. The past emphasis on linear techniques is found to be reasonably valid for the SAM; positive and negative events exhibit approximately equal and opposite responses (Fig. 5). Sea ice relationships with ENSO, by contrast, are found to exhibit substantial nonlinearity, largely due to shifts in the atmospheric wave train between El Niño and La Niña phases (Figs. 6 and 7). The presence of such nonlinearity suggests that, in addition to seasonal considerations, the phase of the ENSO cycle should also be accounted for when diagnosing its relationships to sea ice.
4) *The SAM and ENSO provide a negligible contribution to the linear trends in SIC anomalies over 1980–2008.*
   Consistent with previous studies (Cavalieri and Parkinson 2008; Comiso and Nishio 2008), SIC trends calculated over 1980–2008 are shown to exhibit an out-of-phase relationship between the Bellingshausen and Ross Sea regions (Figs. 8 and 10). Congruency analysis indicates that in a linear sense, trends in the SAM and ENSO are unable to explain a significant component of the observed SIC trends; during DJF SAM-related congruencies peak at $<15\%$ in localized regions (Fig. 9). Such conclusions are consistent with previous studies that both calculate congruency

directly or infer congruency through various mechanisms (Liu et al. 2004; Lefebvre et al. 2004; Sigmond and Fyfe 2010; Schneider et al. 2012). Although ENSO cannot be linearly attributed to SIC trends, ENSO associations with sea ice exhibit a substantial nonlinear component that may have some bearing on low-frequency SIC variability.

This investigation has focused on the contemporaneous relationships between the atmospheric circulation associated with the SAM and ENSO and sea ice during 1980–2008. It was found that, in most circumstances, the dipolar patterns of interannual SIC anomalies associated with the SAM/ENSO are consistent with the anomalous atmospheric circulation centered over the Amundsen Sea. However, the SAM and ENSO also induce significant oceanographic changes to the SH high latitudes that may influence interannual sea ice variability, and perhaps even trends. Holland et al. (2005), for example, demonstrate that ocean conditions are instrumental in forcing the observed SAM/ENSO sea ice dipole, particularly in the Pacific sector. They also note the importance of the ocean in allowing sea ice persistence and advection of anomalies, both of which may have bearing on SIC trends. Such factors were excluded from this study since our focus is on the standing wave components. Nevertheless, given that the ocean exhibits significant variability on interannual–decadal time scales, ocean–sea ice interactions may play a significant role in the SIC variability described here. Furthermore, factors such as ocean temperature trends (Gille 2002, 2008), the poleward migration of the Antarctic Circumpolar Current (Böning et al. 2008), changes to the strength of the subpolar gyres (Wang and Meredith 2008), and ocean freshening (e.g., Rintoul 2007; Zhang 2007; Aiken and England 2008; Liu and Curry 2010) may all have important implications for both the interannual and longer-term variability in Antarctic sea ice.

Acknowledgments. The authors thank the three anonymous reviewers, whose comments greatly helped improve the original manuscript, and Dr. Shayne McGregor for his useful discussions of the results. GRS was supported by a University of New South Wales University International Postgraduate Award. DWJT is supported by the NSF Climate Dynamics program and appreciates sabbatical funding from CCRC, UNSW. This work was also supported by the Australian Research Council.

REFERENCES

Aiken, C. M., and M. H. England, 2008: Sensitivity of the present-day climate to freshwater forcing associated with Antarctic sea ice loss. *J. Climate,* **21,** 3936–3946.

Böning, C. W., A. Dispert, M. Visbeck, S. R. Rintoul, and F. U. Schwarzkopf, 2008: The response of the Antarctic Circumpolar Current to recent climate change. *Nat. Geosci.,* **1,** 864–869.

Bretherton, C. S., M. Widmann, V. P. Dymnikov, J. M. Wallace, and I. Bladé, 1999: The effective number of spatial degrees of freedom of a time-varying field. *J. Climate,* **12,** 1990–2009.

Bromwich, D. H., and R. L. Fogt, 2004: Strong trends in the skill of the ERA-40 and NCEP–NCAR reanalyses in the high and midlatitudes of the Southern Hemisphere, 1958–2001. *J. Climate,* **17,** 4603–4619.

Cavalieri, D. J., and C. L. Parkinson, 2008: Antarctic sea ice variability and trends, 1979–2006. *J. Geophys. Res.,* **113,** C07004, doi:10.1029/2007JC004564.

——, ——, P. Gloersen, J. C. Comiso, and H. J. Zwally, 1999: Deriving long-term time series of sea ice cover from satellite passive-microwave multisensor data sets. *J. Geophys. Res.,* **104** (C7), 15 803–15 814.

Ciasto, L. M., and D. W. J. Thompson, 2008: Observations of large-scale ocean–atmosphere interaction in the Southern Hemisphere. *J. Climate,* **21,** 1244–1259.

Comiso, J. C., and F. Nishio, 2008: Trends in the sea ice cover using enhanced and compatible AMSR-E, SSM/I, and SMMR data. *J. Geophys. Res.,* **113,** C02S07, doi:10.1029/2007JC004257.

Deweaver, E., and S. Nigam, 2002: Linearity in ENSO's atmospheric response. *J. Climate,* **15,** 2446–2461.

Garreaud, R. D., and D. S. Battisti, 1999: Interannual (ENSO) and interdecadal (ENSO-like) variability in the Southern Hemisphere tropospheric circulation. *J. Climate,* **12,** 2113–2123.

Gille, S. T., 2002: Warming of the Southern Ocean since the 1950s. *Science,* **295,** 1275–1278.

——, 2008: Decadal-scale temperature trends in the Southern Hemisphere ocean. *J. Climate,* **21,** 4749–4765.

Goosse, H., W. Lefebvre, A. de Montety, E. Crespin, and A. H. Orsi, 2009: Consistent past half-century trends in the atmosphere, the sea ice and the ocean at high southern latitudes. *Climate Dyn.,* **33,** 999–1016.

Hall, A., and M. Visbeck, 2002: Synchronous variability in the Southern Hemisphere atmosphere, sea ice, and ocean resulting from the annular mode. *J. Climate,* **15,** 3043–3057.

Hartmann, D. L., and F. Lo, 1998: Wave-driven zonal flow vacillation in the Southern Hemisphere. *J. Atmos. Sci.,* **55,** 1303–1315.

Hines, K. M., D. H. Bromwich, and G. J. Marshall, 2000: Artificial surface pressure trends in the NCEP–NCAR reanalysis over the Southern Ocean and Antarctica. *J. Climate,* **13,** 3940–3952.

Holland, M. M., C. M. Bitz, and E. C. Hunke, 2005: Mechanisms forcing an Antarctic dipole in simulated sea ice and surface ocean conditions. *J. Climate,* **18,** 2052–2066.

Hoskins, B. J., and D. J. Karoly, 1981: The steady linear response of a spherical atmosphere to thermal and orographic forcing. *J. Atmos. Sci.,* **38,** 1179–1196.

Jin, D., and B. P. Kirtman, 2009: Why the Southern Hemisphere ENSO responses lead ENSO. *J. Geophys. Res.,* **114,** D23101, doi:10.1029/2009JD012657.

Kalnay, E., and Coauthors, 1996: The NCEP/NCAR 40-Year Reanalysis Project. *Bull. Amer. Meteor. Soc.,* **77,** 437–472.

Karoly, D. J., 1989: Southern Hemisphere circulation features associated with El Niño–Southern Oscillation events. *J. Climate,* **2,** 1239–1252.

——, 1990: The role of transient eddies in low-frequency zonal variations of the Southern Hemisphere circulation. *Tellus,* **42A,** 41–50.

Kistler, R., and Coauthors, 2001: The NCEP–NCAR 50-Year Reanalysis: Monthly means CD-ROM and documentation. *Bull. Amer. Meteor. Soc.,* **82,** 247–267.

Kwok, R., and J. C. Comiso, 2002: Southern Ocean climate and sea ice anomalies associated with the Southern Oscillation. *J. Climate,* **15,** 487–501.

Lefebvre, W., and H. Goosse, 2005: Influence of the southern annular mode on the sea ice-ocean system: The role of the thermal and mechanical forcing. *Ocean Sci.,* **1,** 145–157.

——, ——, R. Timmermann, and T. Fichefet, 2004: Influence of the southern annular mode on the sea ice–ocean system. *J. Geophys. Res.,* **109,** C09005, doi:10.1029/2004JC002403.

L'Heureux, M. L., and D. W. J. Thompson, 2006: Observed relationships between the El Niño–Southern Oscillation and the extratropical zonal-mean circulation. *J. Climate,* **19,** 276–287.

Liu, J., and J. A. Curry, 2010: Accelerated warming of the Southern Ocean and its impacts on the hydrological cycle and sea ice. *Proc. Natl. Acad. Sci. USA,* **107,** 14 987–14 992.

——, ——, and D. G. Martinson, 2004: Interpretation of recent Antarctic sea ice variability. *Geophys. Res. Lett.,* **31,** L02205, doi:10.1029/2003GL018732.

Marshall, G. J., 2002: Trends in Antarctic geopotential height and temperature: A comparison between radiosonde and NCEP–NCAR reanalysis data. *J. Climate,* **15,** 659–674.

——, 2007: Half-century seasonal relationships between the southern annular mode and Antarctic temperatures. *Int. J. Climatol.,* **27,** 373–383.

Mo, K. C., 2000: Relationships between low-frequency variability in the Southern Hemisphere and sea surface temperature anomalies. *J. Climate,* **13,** 3599–3610.

——, and R. W. Higgins, 1998: The Pacific–South American modes and tropical convection during the Southern Hemisphere winter. *Mon. Wea. Rev.,* **126,** 1581–1596.

Nicholls, N., 2008: Recent trends in the seasonal and temporal behaviour of the El Niño–Southern Oscillation. *Geophys. Res. Lett.,* **35,** L19703, doi:10.1029/2008GL034499.

North, G. R., T. L. Bell, R. F. Cahalan, and F. J. Moeng, 1982: Sampling errors in the estimation of empirical orthogonal functions. *Mon. Wea. Rev.,* **110,** 699–706.

Parkinson, C. L., and J. C. Comiso, 2008: Antarctic sea ice parameters from AMSR-E data using two techniques and comparisons with sea ice from SSM/I. *J. Geophys. Res.,* **113,** C02S06, doi:10.1029/2007JC004253.

Raphael, M. N., 2007: The influence of atmospheric zonal wave three on Antarctic sea ice variability. *J. Geophys. Res.,* **112,** D12112, doi:10.1029/2006JD007852.

Rayner, N. A., D. E. Parker, E. B. Horton, C. K. Folland, L. V. Alexander, D. P. Rowell, E. C. Kent, and A. Kaplan, 2003: Global analyses of sea surface temperature, sea ice, and night marine air temperature since the late nineteenth century. *J. Geophys. Res.,* **108,** 4407, doi:10.1029/2002JD002670.

Renwick, J. A., 2002: Southern Hemisphere circulation and relations with sea ice and sea surface temperature. *J. Climate,* **15,** 3058–3068.

Rintoul, S. R., 2007: Rapid freshening of Antarctic Bottom Water formed in the Indian and Pacific Oceans. *Geophys. Res. Lett.,* **34,** L06606, doi:10.1029/2006GL028550.

Santer, B. D., T. M. L. Wigley, J. S. Boyle, D. J. Gaffen, J. J. Hnilo, D. Nychka, D. E. Parker, and K. E. Taylor, 2000: Statistical significance of trends and trend differences in layer-average atmospheric temperature time series. *J. Geophys. Res.,* **105** (D6), 7337–7356.

Schneider, D. P., C. Deser, and Y. Okumura, 2012: An assessment and interpretation of the observed warming of West Antarctica in the austral spring. *Climate Dyn.,* **38,** 323–347, doi:10.1007/s00382-010-0985-x.

Sen Gupta, A., and M. H. England, 2006: Coupled ocean–atmosphere–ice response to variations in the southern annular mode. *J. Climate,* **19,** 4457–4486.

Sigmond, M., and J. C. Fyfe, 2010: Has the ozone hole contributed to increased Antarctic sea ice extent. *Geophys. Res. Lett.,* **37,** L18502, doi:10.1029/2010GL044301.

Simmonds, I., and T. H. Jacka, 1995: Relationships between the interannual variability of Antarctic sea ice and the Southern Oscillation. *J. Climate,* **8,** 637–648.

Stammerjohn, S. E., D. G. Martinson, R. C. Smith, X. Yuan, and D. Rind, 2008: Trends in Antarctic annual sea ice retreat and advance and their relation to El Niño–Southern Oscillation and southern annular mode variability. *J. Geophys. Res.,* **113,** C03S90, doi:10.1029/2007JC004269.

Stroeve, J., M. M. Holland, W. Meier, T. Scambos, and M. Serreze, 2007: Arctic sea ice decline: Faster than forecast. *Geophys. Res. Lett.,* **34,** L09501, doi:10.1029/2007GL029703.

Thompson, D. W. J., and J. M. Wallace, 2000: Annular modes in the extratropical circulation. Part I: Month-to-month variability. *J. Climate,* **13,** 1000–1016.

——, and S. Solomon, 2002: Interpretation of recent Southern Hemisphere climate change. *Science,* **296,** 895–899.

Turner, J., and Coauthors, 2009: Non-annular atmospheric circulation change induced by stratospheric ozone depletion and its role in the recent increase of Antarctic sea ice extent. *Geophys. Res. Lett.,* **36,** L08502, doi:10.1029/2009GL037524.

Wang, Z., and M. P. Meredith, 2008: Density-driven Southern Hemisphere subpolar gyres in coupled climate models. *Geophys. Res. Lett.,* **35,** L14608, doi:10.1029/2008GL034344.

Yuan, X., and D. G. Martinson, 2000: Antarctic sea ice extent variability and its global connectivity. *J. Climate,* **13,** 1697–1717.

——, and C. Li, 2008: Climate modes in southern high latitudes and their impacts on Antarctic sea ice. *J. Geophys. Res.,* **113,** C06S91, doi:10.1029/2006JC004067.

Zhang, J., 2007: Increasing Antarctic sea ice under warming atmospheric and oceanic conditions. *J. Climate,* **20,** 2515–2529.